

Article

Point Cloud Based Mapping of Understory Shrub Fuel Distribution, Estimation of Fuel Consumption and Relationship to Pyrolysis Gas Emissions on Experimental Prescribed Burns [†]

Molly M. Herzog ¹, Andrew T. Hudak ², David R. Weise ³, Ashley M. Bradley ¹, Russell G. Tonkyn ¹, Catherine A. Banach ¹, Tanya L. Myers ¹, Benjamin C. Bright ², Jonathan L. Batchelor ⁴, Akira Kato ⁵, John S. Maitland ⁶ and Timothy J. Johnson ^{1,*}

¹ Chemical Physics and Analysis, Pacific Northwest National Laboratory, Richland, WA 99354, USA

² USDA Forest Service, Rocky Mountain Research Station, Moscow, ID 83843, USA

³ USDA Forest Service, Pacific Southwest Research Station, Riverside, CA 92507, USA

⁴ School of Environmental and Forest Sciences, University of Washington, Seattle, WA 98195, USA

⁵ Graduate School of Horticulture, Chiba University, Chiba 271-8510, Japan

⁶ Fort Jackson Forestry Branch, Ft. Jackson, Columbia, SC 29207, USA

* Correspondence: timothy.johnson@pnnl.gov

[†] This manuscript was produced, in part, by U.S. Government employees on official time, is not subject to copyright and is in the public domain.



Citation: Herzog, M.M.; Hudak, A.T.; Weise, D.R.; Bradley, A.M.; Tonkyn, R.G.; Banach, C.A.; Myers, T.L.; Bright, B.C.; Batchelor, J.L.; Kato, A.; et al. Point Cloud Based Mapping of Understory Shrub Fuel Distribution, Estimation of Fuel Consumption and Relationship to Pyrolysis Gas Emissions on Experimental Prescribed Burns. *Fire* **2022**, *5*, 118. <https://doi.org/10.3390/fire5040118>

Academic Editor: James A. Lutz

Received: 8 July 2022

Accepted: 10 August 2022

Published: 16 August 2022

Publisher's Note: MDPI stays neutral with regard to jurisdictional claims in published maps and institutional affiliations.



Copyright: © 2022 by the authors. Licensee MDPI, Basel, Switzerland. This article is an open access article distributed under the terms and conditions of the Creative Commons Attribution (CC BY) license (<https://creativecommons.org/licenses/by/4.0/>).

Abstract: Forest fires spread via production and combustion of pyrolysis gases in the understory. The goal of the present paper is to understand the spatial location, distribution, and fraction (relative to the overstory) of understory plants, in this case, sparkleberry shrub, namely its degree of understory consumption upon burn, and to search for correlations between the degree of shrub consumption to the composition of emitted pyrolysis gases. Data were collected in situ at seven small experimental prescribed burns at Ft. Jackson, an army base in South Carolina, USA. Using airborne laser scanning (ALS) to map overstory tree crowns and terrestrial laser scanning (TLS) to characterize understory shrub fuel density, both pre- and postburn estimates of sparkleberry coverage were obtained. Sparkleberry clump polygons were manually digitized from a UAV-derived orthoimage of the understory and intersected with the TLS point cloud-derived rasters of pre- and postburn shrub fuel bulk density; these were compared in relation to overstory crown cover as well as to ground truth. Shrub fuel consumption was estimated from the digitized images; sparkleberry clump distributions were generally found to not correlate well to the overstory tree crowns, suggesting it is shade-tolerant. Moreover, no relationship was found between the magnitude of the fuel consumption and the chemical composition of pyrolysis gases, even though mixing ratios of 25 individual gases were measured.

Keywords: pyrolysis; remote sensing; point cloud; understory spatial distribution; sparkleberry; understory consumption; airborne laser scanning; terrestrial laser scanning; infrared; FTIR

1. Introduction

Prescribed fire is used in the United States and throughout the world today as an effective land management tool [1,2]. Prescribed fire and wildland fire are two examples of biomass burning; heating, cooking, transportation and power generation are other known types [3]. All forms of biomass burning produce aerosols and greenhouse gases, particularly the small gaseous molecules CO and CO₂ [4,5]. The gases and aerosols produced from biomass burning depend on the loading and composition of the source fuels as well as multiple environmental factors. An improved quantitative understanding of the dependencies is needed, particularly knowledge of the initial and final gas compositions released into the plume and how these depend on the fuel loads (quantity) and fuel composition

(quality). In the U.S., since the advent of the 1970 Clean Air Act, numerous studies and research programs have sought to understand these dependencies, including laboratory studies of gaseous emissions [5–8], as well as studies that delineate the emissions as per the phase of the fire, e.g., combustion vs. smoldering [8].

Biomass burning typically involves multiple chemical and physical processes that occur over a wide range of temperatures and over different time scales: evaporation, pyrolysis, gas combustion, and char oxidation, which leads to smoldering combustion [9]. One of the early processes is pyrolysis, the thermal breakdown of solid fuels such as lignin, cellulose, or hemi-cellulose into gas-phase molecules [10]. The pyrolysis process continues throughout the course of the burn, and pyrolysis gases are what oxidize to produce the flame, which is visible to the eye due to the glowing carbon in the flame. Flaming combustion is the hottest phase, with peak temperatures ranging from 600 °C to as high as 1000 °C; this phase entails rapid oxidation reactions of the gases emitted from the solid fuel, with primary flaming products being CO₂, H₂O, NO_x, and SO₂ gases along with carbon soot [11]. Smoldering combustion follows the flaming stage and involves surface oxidation via “glowing” (~400 to 800 °C), which produces enhanced levels of CO, CH₄, NH₃, nonmethane organic carbon (NMOC), and aerosols as compared to the flaming phase due to reduced oxidation rates at lower temperatures [12]; the smoldering phase can last several hours to days or even weeks for certain types of fuel (stumps, logs, organic soils, peat, and coal) [13].

Experiments to study biomass burning range from small-scale controlled laboratory experiments [14,15] to larger-scale laboratory burns [16], and even to prescribed outdoor burns at the stand and landscape levels: Both Scharko et al. [17] and Akagi et al. [18] have reported such studies using infrared methods, in extractive and open-path modes, respectively. Burling et al. [19] also used infrared methods, but included airborne measurements as well, whereas Gilman and co-workers focused on the air quality impacts of volatile organic compounds [17–20]. Many previous works have detected and identified dozens of trace gases emitted from biomass burning [11,21,22]. The present effort is part of a larger five-year study to better understand the mechanisms and conditions of pyrolysis associated with prescribed fire. In particular, we are working to understand both the physics and chemistry of the pyrolysis phase at the early stages of the burning process [8,18]. During the course of these studies, we have used different methods, including both time-resolved and static infrared spectroscopy [17,18,23], to characterize gaseous pyrolysis products via the measurement of a variety of live and dead foliar fuel particles (measure and identify pyrolysis products in lab and small-scale field experiments) and thus improve our ability to model the pyrolysis and ignition processes. The results of the field and laboratory measurements are ultimately integrated into models to identify potential improvements that can enhance our understanding of pyrolysis and ignition in wildland fuels. For prescribed fire in particular, key input parameters for better quantification include the composition, identity, species, and environmental conditions of the understory [24]. While crown fires may consume overstory forest canopies, most prescribed fires are designed to burn only the accumulated dead organic material (litter, duff), surface fuels (down woody debris), and understory shrubs and trees [25]. In most cases, determining the fuel consumption still requires the time-intensive method of the ground-based sampling of understory fuels via destructive methods both before and after a prescribed burn (e.g., Southeastern Forest Experiment Station (Asheville, NC, USA) and Southern Forest Experiment Station (New Orleans, LA, USA) 1959) [26].

The present study has two components. First, we mapped the density and distribution of understory shrub fuels consumed by prescribed fire during the growing season at a series of prescribed fires conducted on a military base in the southeastern U.S. In a previous study, results from 3D point cloud analysis techniques were compared to results from traditional sampling techniques to estimate shrub fuel bulk density [27]. Specifically, point cloud data from terrestrial laser scanning (TLS) were collected pre- and postburn to estimate understory shrub fuel bulk density, thus enabling an estimation of shrub fuel

consumption. Building upon that study, this study applied another existing methodology to map overstory tree crown cover as object polygons from airborne laser scanning (ALS) point cloud data. In addition, point cloud data derived from Unoccupied Aerial Vehicle (UAV) imagery, using Structure from Motion (SfM) technology, were used to generate orthographically corrected images of vegetation less than 2 m in height. The images were used to digitally delineate individual shrubs and shrub clumps as fuel objects. As with the TLS, the UAV datasets were collected immediately before and after the burn, enabling the mapping of pre- and postburn shrub fuel object distributions, such that their consumption by fire could be mapped. The wealth of point cloud information thus assembled to map fuel consumption provided for the second component of the study, namely to relate fuel consumption to gases pyrolyzed by the fire. Understanding the composition and quantity of the pyrolysis gases produced by the shrub component in these forested stands provides the information that can be used in physically based fire models that include the chemistry of the combustion reactions, thus allowing us to model these fires more realistically. For all the burn plots studied here, the shrub understory is dominated by two species, namely sparkleberry (*Vaccinium arboreum* Marshall), and turkey oak (*Quercus laevis* Walter). Sparkleberry, a deciduous shrub, can have a significant impact on the fire behavior that occurs in these forests by increasing the flame lengths when it ignites, resulting in greater heat release, spread rates, and potential damage to the overstory. While two previous studies [23,28] have indicated that certain gases such as phenol may be a characteristic gas of such berry plants upon pyrolysis (sparkleberry is a member of the *Vaccinium* genus), there are few other reports toward this end. While sparkleberry foliage obviously does not burn during the dormant season (no leaves), it does burn in the early growing season, i.e., after leaf-out. For this reason, and also for safety reasons, the burns were conducted only in the early growing season at Ft. Jackson.

Using modern point cloud-based remote sensing methods, the goal of the present work is thus to understand the spatial location, distribution and fractional coverage (relative to the overstory) of the sparkleberry shrub understory, and the degree of understory consumption upon burning, and, ultimately, to use these data to uncover possible correlations between the degree of shrub consumption and the chemical composition of the emitted pyrolysis gases. Our approach is thus composed of four discrete steps, namely: (1) analyze the locations and fraction of sparkleberry shrubs in relation to the tree crowns, (2) compare the digitized sparkleberry shrub clumps to independent ground truth measurements of sparkleberry coverage, (3) calculate estimated fuel consumption from both the digitized sparkleberry clumps and the ground truth measurements of sparkleberry coverage, and (4) attempt to correlate fuel consumption estimates to the composition of the collected pyrolysis gases. The last step is premised on the known flammability of sparkleberry shrubs early in the growing season, i.e., it is anticipated that experimental burn units with greater sparkleberry coverage will emit greater quantity and diversity (in terms of chemical composition) of pyrolysis gases. While sparkleberry is a representative understory plant for many ecosystems in eastern North America, an ancillary goal of the work is to develop the methodologies such that they can be applied to other ecosystems.

2. Methods

2.1. Study Area

A series of prescribed burns was conducted in spring of 2018 at the U.S. Army's Fort Jackson. Located adjacent to Columbia, South Carolina (SC), the base covers approximately 53,000 acres in the Carolina sandhills, an ecological region of the southeastern United States characterized by well-drained, nutrient poor soil and frequent fire activity [29]. The forests of the Sandhills region are composed of a variety of vegetation well-adapted to these conditions. At Ft. Jackson, species present in the overstory layer include longleaf pine (*Pinus palustris* Mill.) and loblolly pine (*P. taeda* L.), while the understory layer is composed primarily of turkey oak and sparkleberry; experimental burn plots were selected for having ample coverage of sparkleberry, the principal shrub species of interest for this

study (Figure 1). In addition to controlling the understory to facilitate military training, prescribed burns assist in species management, specifically promoting the regeneration and growth of longleaf pine, once a primary component of the southeastern U.S. pine forest ecosystem, and maintaining habitat for animal species of concern such as the red-cockaded woodpecker (*Dryobates borealis*) [30].



Figure 1. Vegetation of the Carolina sandhills ecological region at Ft. Jackson: (a) view of over-story longleaf and loblolly pine trees from ground level; (b) longleaf pine seedling in grass stage; (c) understory view of turkey oak and sparkleberry; (d) close-up view of sparkleberry foliage.

Seven burn units, designated as 16D1, 16D5, 16D6, 24A Main, 24A Triangle, 24B Main, and 24B Triangle, were selected due to having a significant sparkleberry component in their understory vegetation (Figure 2). Areas with significant sparkleberry coverage were preferred due to interest in the pyrolysis gases produced from burning sparkleberry during its growing season [17,23,28]. Each unit was approximately 0.16 hectares in area; the units were delimited by fresh bulldozer tracks, which served both as visible boundaries around each unit and also as firebreaks to prevent the spread of fire outside the units. Units 16D1, 16D5, and 16D6 were approximately square in shape, while the Units 24A and 24B were more irregularly shaped, with each larger main unit situated adjacent to a smaller triangle unit.

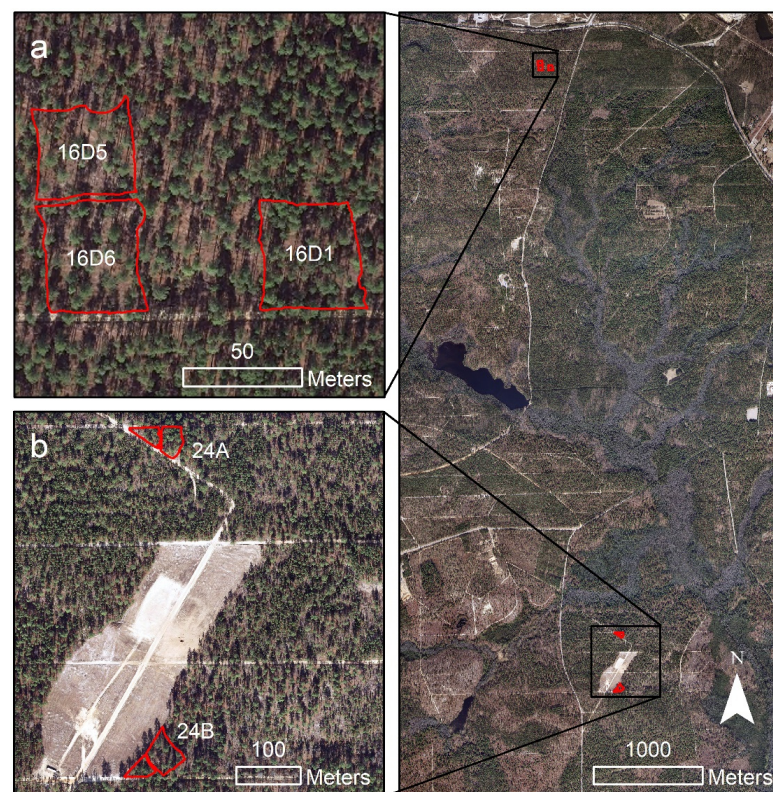


Figure 2. Location of individual burn plots at Ft. Jackson showing experimental burn units in management areas (a) 16D and (b) 24A and 24B.

2.2. In Situ Data Collection and Preparation

2.2.1. Airborne Laser Scanning

Airborne laser scanning is a LiDAR measurement system taken from a plane or UAV. ALS is useful at distinguishing between canopy-level and ground-level features. ALS measurements can determine the height of individual tree crowns [31] as well as density and canopy cover due to the 3D nature of the data [32]. The ALS data used in this study were collected in November 2015 with an Optech ALTM Gemini sensor at an average density of $8.7 \text{ points m}^{-2}$ [27]. The use of trade or firm names in this publication is for reader information and does not imply endorsement by the U.S. Department of Agriculture of any product or service.

The ALS data served two purposes in this study: The first purpose was to use the georectified ALS point clouds as base data to which TLS and UAV point clouds were co-registered; the tree crowns provided useful features for accurate co-registration. The second was to interpolate a canopy height model (CHM) surface of 1-m resolution from the ALS point cloud. The CHM was used to identify and segment individual tree crown objects from the CHM and export the resulting 2D crown polygons as a shapefile (Figure 3).

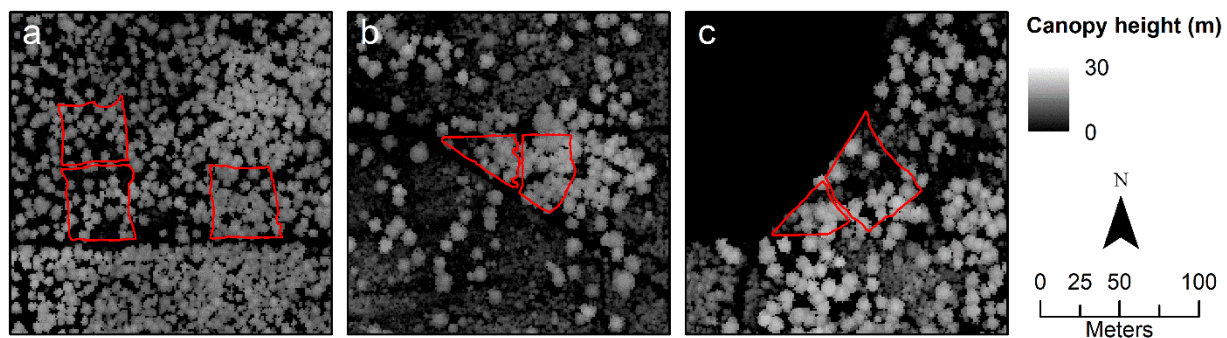


Figure 3. Canopy height model (CHM) derived from ALS at 1-m resolution, depicting overviews of burn units (a) 16D1, 16D5, and 16D6, (b) 24A Triangle and 24A Main, and (c) 24B Triangle and 24B Main.

2.2.2. Terrestrial Laser Scanning

Terrestrial laser scanning is a second LiDAR measurement method in which data are taken from discrete locations at ground level rather than from above the canopy while in motion; this allows for the higher precision measurements of fuel bed volume at discrete locations [33]. The TLS can be mounted on a tripod or attached to a boom lift and can complete several scans of an area from a horizontal or low oblique angle, whose data can be merged to form one set of point cloud data [27]. The TLS sensor used in this study was an LMS 511 (SICK Inc., Waldkirch, Germany), and data were collected at each unit in the days just prior to, and immediately after, burning.

The TLS data were used to create a model for determining prefire and postfire fuel densities, from which estimates for fuel consumption were derived by comparing the prefire and postfire density maps, as previously described [27]. In brief, the TLS point clouds, merged from multiple scans, were delineated into $0.1 \times 0.1 \times 0.1 \text{ m}^3$ voxels (3-dimensional pixels), populated in a binary manner with a 1 if fuel was present (as indicated by shrub returns) and 0 if no fuel was present. In order to determine the mass density associated with each voxel, a $0.5 \times 0.5 \times 2 \text{ m}^3$ plot was established in each burn unit for comparison of the TLS to the destructive sampling. The 3D shrub plots (each marked by metal conduits) were identified in the TLS point cloud data; within the $0.5 \times 0.5 \times 2 \text{ m}^3$ area of each plot, the voxels where fuel was indicated to be present were summed. The occupied voxel density of each 3D shrub plot was then compared to the shrub biomass densities determined through traditional destructive sampling; a logarithmic model was fit to relate occupied voxel density to actual mass density. This model was applied to occupied voxel density rasterized across each entire burn unit, pre- and postburn, from 0.0 to 2.0 m above ground. These resulting pre- and postburn rasters had a resolution of 1.0 m, where

pixel values represent estimated shrub fuel density in g/m^3 (Figure 4) [27]. Subtracting the postburn raster from the preburn raster yielded a raster which represented the estimated shrub fuel density consumed during each burn. The consumption rasters were used to estimate the fuel consumption within visible fuel objects (e.g., sparkleberry shrub clumps) explicitly digitized from UAV imagery, as described in the next subsection.

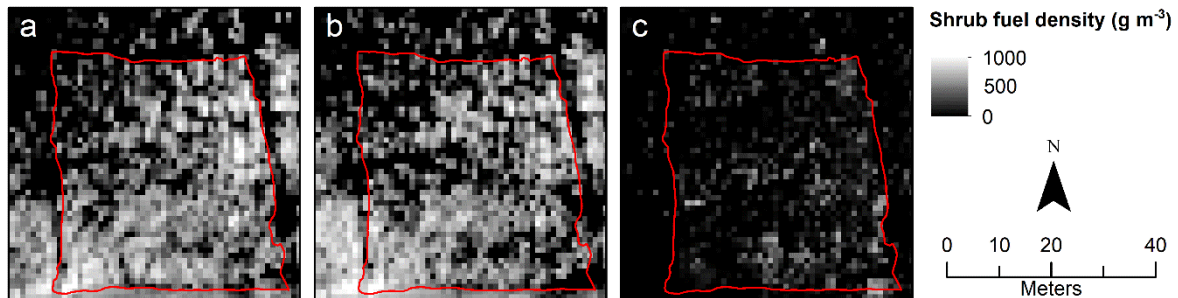


Figure 4. Fuel density rasters for unit 16D1 derived from TLS point cloud data at 1 m resolution and depicting (a) prefire fuel density, (b) postfire fuel density, and, by difference, (c) consumed fuel density. If estimated consumption was less than 0, it was assigned a value of 0.

2.2.3. Unmanned Aerial Vehicle Imagery

Images were taken at a variety of angles from an Unmanned Aerial Vehicle (UAV-Marvic Pro) quadcopter (DJI, Inc., Shenzhen, China) flown in the days just prior to and after the burns were conducted. For image acquisition, transects were flown over plots at 61 and 122 m height above ground (Figure 3). Images were collected with 80% front and side overlap using the stock 12-megapixel RGB camera with a pixel resolution of 3 cm at 100 m above ground. The RGB imagery provided a nadir view of each burn unit and, being higher resolution (0.06 m), served as the source imagery from which the individual sparkleberry shrubs or shrub clumps were manually digitized. The original images contained the canopy layer, which made it difficult to identify individual sparkleberry bushes. In order to obtain an improved view of the understory, images taken from the UAV were altered by digitally removing obstructions caused by the tree canopy layer. Image processing was performed using the Agisoft program Photoscan. Multiple images taken at a variety of oblique angles were merged using Structure from Motion technology to create 3D point clouds [34,35]. Photogrammetric point clouds were created using 120 to 240 photos for each plot, resulting in a pixel resolution of 1 to 2 cm. The point clouds derived from the UAV imagery allowed for the separation of points above and below 2 m in height above ground. Points above 2 m (i.e., tree crowns) were digitally removed from the images; points below 2 m were subsequently rasterized into an orthoimage of the understory ground in each burn unit at a resolution of 0.06 m (Figure 5). The 2-m level was chosen since the sparkleberry shrubs only achieve plant heights up to 2 m above ground and because the majority of tree crowns were greater than 2 m off the ground [27]. Understory shrubs were visible in the orthoimage after overstory removal, albeit with a degree of obscuration, especially within the residual tree shadows, which likely varied in linear proportion to tree canopy cover [36].

2.2.4. Field Data

Around the perimeter of each burn unit, several gas canisters were filled at marked locations in order to relate estimated sparkleberry shrub coverage to collected pyrolysis-phase gas emissions; the details of the IR gas analysis methods are described in detail elsewhere [17,23].

Destructive sampling of pre- and postburn fuels was conducted within four of the burn units (16D1, 16D5, 24A Main, 24B Main); this was necessary to relate measured shrub fuel biomass density to occupied voxel density derived from the TLS point clouds, resulting in the shrub fuel biomass density maps used in this study; details are provided elsewhere [27].

In the fall of 2020, sparkleberry shrub coverage was estimated in the field at the 24A and 24B units. The purpose was to independently estimate the current coverage and distribution of sparkleberry bushes, which, after being given 2 years to resprout and recover, was expected to have returned to approximate preburn conditions. However, it seemed unreasonable to expect individual shrub clumps to recover to their previous size and shape. Therefore, for each burn unit, percent coverage of consistently spaced sparkleberry clumps was estimated within a broader radius around a recorded centerpoint location. The radius and percent cover were stored as attributes for each individual point.

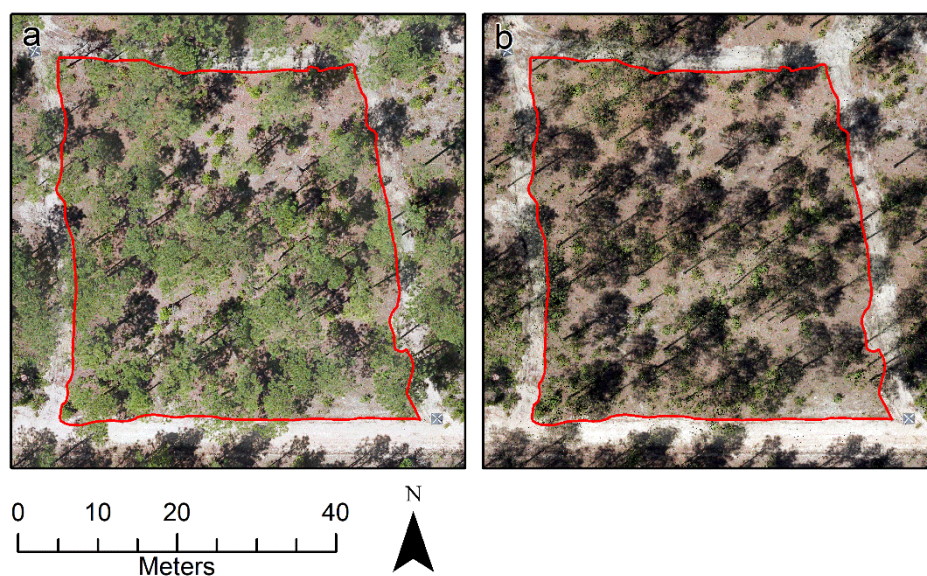


Figure 5. UAV imagery of unit 16D1 captured in RGB (a) prior to digital removal of tree crowns and (b) after digital removal of tree crowns. Dark regions in (b) are largely tree shadows which remain.

2.3. Digitization of Fuel Sources

2.3.1. Digitization

Individual fuel objects were manually digitized using ArcGIS software. The 0–2 m RGB orthoimagery for each individual burn unit, both pre- and postburn, was uploaded into the software. By manually plotting points to trace the perimeter of specific features, the software automatically connects the line between points and forms polygons. The software also recognizes lines (unclosed polygons) or individual points. Using the 0–2 m imagery, which provided an unobstructed view of the understory, each individual feature was thus delineated, and the collection of polygons for each burn unit was saved as a shapefile.

Features of interest include the unit borders, burned logs, and sparkleberry shrubs (Figure 6). The boundaries of each unit (bulldozer lines) also required digitization to accurately determine the burn unit areas. Downed logs and their postburn ash relics (known as ghost logs) were also digitized because such downed woody debris contributes heavily to smoldering smoke; the degree to which the few burning logs affected pyrolysis gas measurements is unknown but is believed to be negligible. Being the primary focus of this study, the sparkleberry shrubs were digitized with greatest care. Each burn unit contained between 100 and 400 individual sparkleberry bushes or consolidated clumps. Large patches of sparkleberry were digitized into individual shrub polygons from which they could be visually resolved.

An additional attribute was added to the preburn sparkleberry shapefiles, which indicates that the confidence level that the regions delineated accurately represent sparkleberry shrub coverage. The confidence attribute was assigned on a simple 1 to 3 digital scale of low, medium, and high confidence, where high meant that finding sparkleberry within the marked region was highly probable, while low meant there was more uncertainty that the identified feature was indeed sparkleberry (Figure 7a). The assignments of the confidence attribute were not rooted in numerical calculation of uncertainty; they were based on visual

appraisal by a single interpreter and are thus somewhat subjective, yet were consistently assigned across all seven burn units.

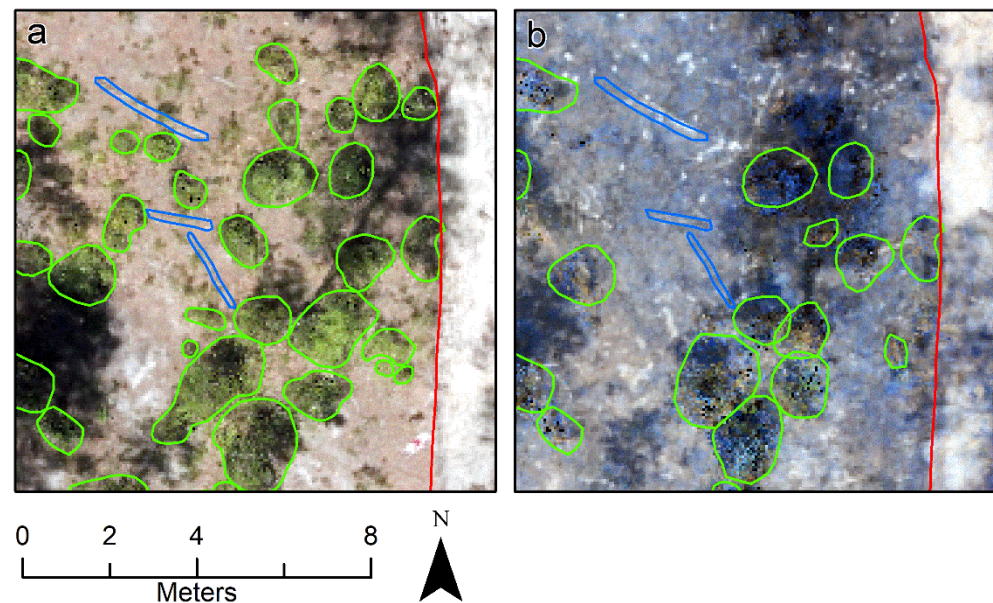


Figure 6. Examples of digitized sparkleberry (in green) and downed/burned logs (in blue) from burn unit 16D5, (a) prefire and (b) postfire. The red line depicts the east edge of the burn unit, bounded by the brighter bulldozer line to the east.

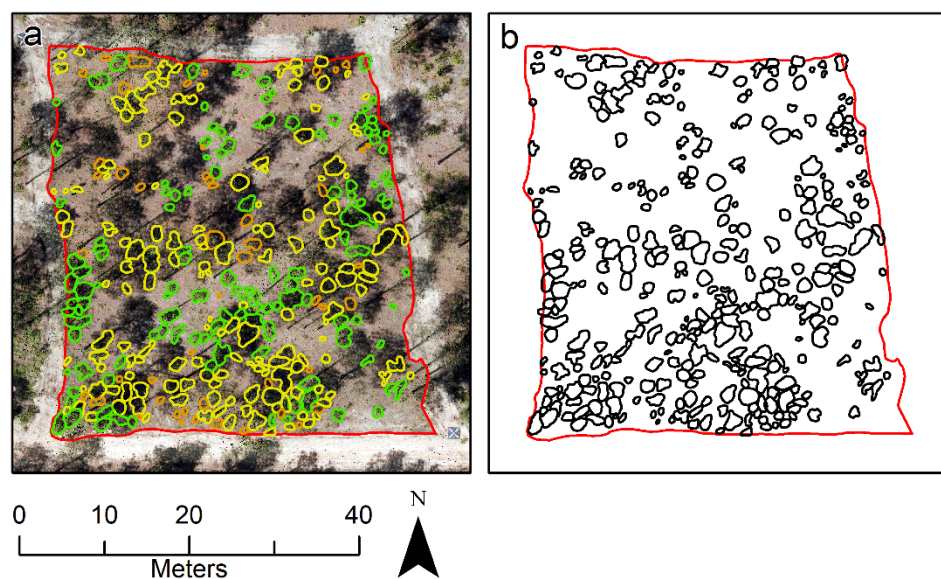


Figure 7. (a) Sparkleberry confidence metric expressed in unit 16D1 with color coding (high-confidence = green, medium-confidence = yellow, low-confidence = orange). (b) All sparkleberry clump polygons digitized in unit 16D1, depicting the areal coverage and distribution of shrub clumps.

2.3.2. Rasterization

Once the sparkleberry features in each burn unit were digitized and collectively saved as a shapefile, each shapefile was converted into an indexed raster using the statistical computing software R [37]; pixels of the associated raster which fell within the boundaries of a polygon were indexed as “1”, and pixels which fell outside of the polygons were indexed as “0” (Figure 7b). The resolution of the sparkleberry raster was set to 1.0 m to match the fuel density rasters generated from the TLS. The transformation from a vector shapefile to an indexed raster simplified data extraction from prefire, postfire, and consumption fuel density

rasters. The manual conversion between vector and raster formats here and elsewhere in this analysis caused only negligible differences (all within $\pm 1 \text{ m}^2$) in areal extents.

2.4. Ground Truth Measurements

Using ArcMap, each individual coordinate point was buffered using the recorded radius to create circular polygons which was an efficient means with which to describe the location and coverage of sparkleberry in the field within each burn unit. To avoid the duplication of data in regions where buffered circles overlapped, a line was drawn along the major axis of the overlap area to bisect the region between the overlapping polygons (Figure 8), such that the two competing cover estimates were each assigned to half of the overlap region.

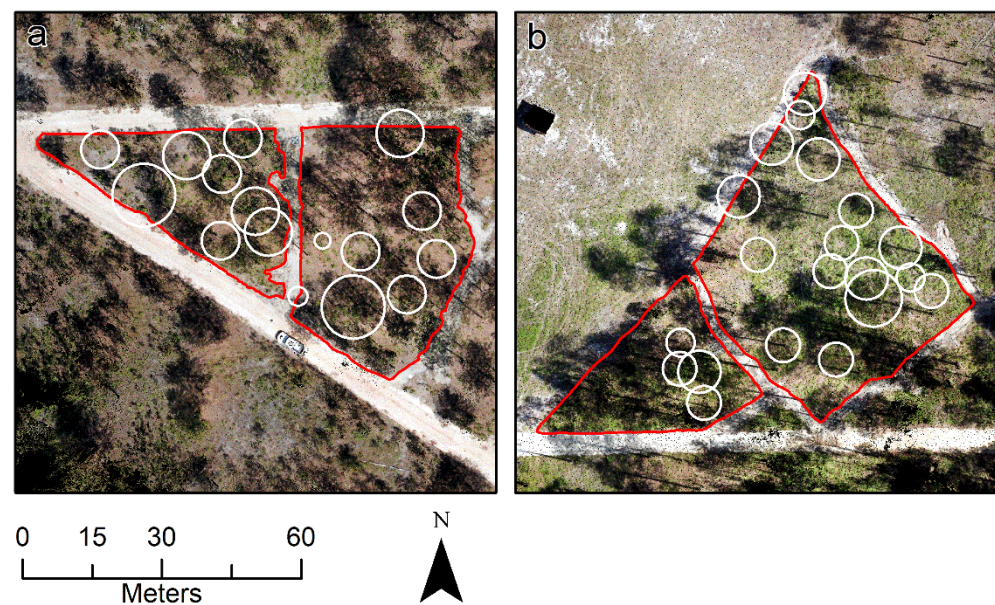


Figure 8. Buffered polygons, adjusted for overlap, representing ground truth estimates of sparkleberry cover distributions for burn units (a) 24A and (b) 24B. Portions of polygons extending outside a burn unit were truncated at the boundary.

The polygons of each unit were collectively saved as a shapefile in ArcMap, imported into R, and converted into a raster. Due to the limited precision of GPS under the forest canopy, the precision of both the ground truth measurements and the derived rasters was limited to 1 m. Similar to the digitized sparkleberry, the ground truth raster was converted into an indexed raster, where pixels located within the polygons were indexed as “1” and pixels outside of the polygons were indexed as “0”.

2.5. Fourier Transform Infrared (FTIR) Spectroscopy Gas Analysis

A 3 L Summa canister was filled with gases from five of the seven burn plots, resulting in five canister samples. The sampling probe collected gases near the base of the flame just prior to flame arrival to capture pyrolysis gases [17,38]. The 7–10 aliquots collected from each plot were collected from multiple locations with a portion of the plot near the sparkleberry clumps; however, the composite sample represented the plot and was not spatially linked to a particular clump of plants. The gas contents of the canisters were analyzed in the laboratory using an 8-m White cell (Bruker A136/2-L) coupled to a Bruker Tensor 37 FTIR spectrometer, as previously described [17,23]. The spectrometer was purged with dry air from a gas generator and the entire system was heated to 70 °C to prevent adhesion of compounds to the stainless-steel tubing. From the five canisters that were collected, one to three gas samples were extracted and injected into the White cell for a total of ten gas compositions. Spectra were analyzed using the MALT5 program, along with 50 °C reference spectra from the PNNL database [39,40] and absorption lines from

HITRAN in regions where H₂O and CO₂ were not saturated [41]. Mixing ratios of pyrolysis gases were determined in ppm_v.

2.6. Statistical Analysis

Statistical analysis was used to help achieve all four study objectives: (1) analyze the locations of sparkleberry shrubs in relation to tree crowns, (2) compare the sparkleberry clump digitizations to independent ground truth measurements of sparkleberry coverage, (3) calculate estimated fuel consumption from both the digitized sparkleberry clumps and the ground truth measurements of sparkleberry coverage, and (4) relate fuel consumption estimates to the composition of pyrolyzed gases collected. While ArcMap was used for creating, editing, and georeferencing images and shapefiles, most of the spatial analysis was conducted using the statistical computing software R [37]. Analysis methods are discussed in turn.

2.6.1. Tree Crowns vs. Sparkleberry Clumps Distribution

The purpose of analyzing the overlap between tree crowns and sparkleberry clumps was to determine whether there was an association between the location of sparkleberry plants and the location of the tree crowns. Sparkleberry is shade-tolerant [42] and is described as growing best in direct sunlight to partial shade [43]. We had hypothesized that more sparkleberry plants would be located in the area between tree crowns due to greater sunlight. In order to test this relationship, the sparkleberry clump shapefiles and tree crown shapefiles were intersected to determine the amount of overlap. If the sparkleberry favored sunlight, the overlap area should be small relative to the total sparkleberry area (relatively less sparkleberry cover under tree crowns). Using the observations of estimated overlap from the 7 burn units, a one-sided *t*-test was performed to test if the overlap proportion was less than 0.5. While this is a relatively small sample size, the *t*-test has been shown to be a reliable statistic yielding acceptable power for small sample sizes [44].

2.6.2. Ground Truth Measurements

The ground truth measurements of sparkleberry coverage, taken in units 24A and 24B, were expressed as percent cover. An area-weighted geometric mean for sparkleberry cover was estimated using

$$\bar{x} = \left(\prod_{i=1}^n x_i^{w_i} \right)^{1/\sum_{i=1}^n w_i} = \exp \left(\frac{\sum_{i=1}^n w_i \ln x_i}{\sum_{i=1}^n w_i} \right)$$

where x_i is the percent cover and w_i is the area of the polygon. The polygons were not perfect circles; the area of individual polygons and their total sum were therefore calculated geometrically in ArcMap, rather than using the buffer radius to calculate area. Polygons that extended beyond the perimeter of the units were cropped using the border shapefile. Once the weighted geometric mean was determined and the total polygon area calculated, the mean percentage was applied to the total area of polygons to estimate what area of the burn units was covered with sparkleberry. A two-sample *t*-test compared the digitized sparkleberry area with the ground truth measurement for four of the burn units. Ground truth measurements of sparkleberry cover were not available for three of the seven burn units; a simple linear regression was fitted to predict ground truth shrub fuel loading from shrub fuel loading estimated within the digitized sparkleberry clumps aggregated within these burn units.

2.6.3. Fuel Density/Consumption Estimates

To estimate consumption, the shapefiles within each burn unit were split into two subsets: one inside sparkleberry clumps and the complement outside sparkleberry clumps. The shapefiles were superimposed on the prefire, postfire, and consumption rasters generated from the TLS, and the density values from these rasters were extracted from within

the areas of the shapefiles. Both the fuel density rasters and the shapefiles were cropped to the boundaries of the unit to ensure that values outside of the burn areas would not be included in the analysis. The arithmetic mean fuel density for each subset was multiplied by the area of each subset to determine an estimate for the total fuel consumption for each burn unit.

2.6.4. Effect of Fuel Consumption on Composition of Pyrolysis Gases

As part of the overall study, identifying and quantifying the composition of pyrolysis gas emissions associated with the prescribed burning of the plots was measured and determined using FTIR spectroscopy [23]. We have shown elsewhere that the gases associated with wildland fire are a type of data that are amenable to the application of specialized statistical techniques [45–48]. An important characteristic of compositional data is that these multivariate data are relative, and the information is contained in the ratios of the different gases in the composition.

Common practice to analyze compositional data is to transform the data using the isometric log-ratio (*ilr*) transformation and then apply familiar statistical techniques (such as linear regression, analysis of variance, etc.) to the transformed data [49]. For this study, the measured gas composition contained 25 gas mixing ratios expressed in ppm. For three of the five canisters with multiple subsamples, the geometric mean of the concentration was calculated for each gas. Isoprene was not detected in one of the samples, therefore a method to replace below-detection limit values (BDL) with a non-zero value was used [50,51]. Compositional data are typically normalized (closed) to place on a relative scale [45], and these data are used to calculate mole fractions, mass fractions, and mixing ratios [52]. A generic *ilr* transformation of the closed concentrations yielded 24 real-valued multivariate coordinates. While it is possible to develop individual linear regressions to test the significance of the relationship between fuel consumption and the relative amount of each gas, interpreting these individual regressions is difficult since the dependent variable (*Y*) is a log-ratio of 2 or more of the gases. The small sample size (5) precluded testing the transformed concentrations for multivariate normality. Permutational multivariate analysis of variance (PERMANOVA) tested the significance of the relationship between the predictor variable fuel consumption and the dependent multivariate gas composition [53,54] Equation (1) where *ilr* denotes the isometric log-ratio transformation, *Y* is the vector of 24 *ilr* coefficients from the 25 gases, and *a* and *b* are the intercept and slope vectors [55], each containing 24 values. This approach was also used because there were fewer observations (only five) compared to the number of gases (25), which is problematic for classical multivariate analysis of variance, which assumes multivariate normality and more observations than gases. PERMANOVA tests the same hypotheses as a MANOVA would in a distribution-free setting using permutational algorithms [56].

$$\text{ilr}(\mathbf{Y}_i) = \text{ilr}(\mathbf{a}) + X_i \text{ilr}(\mathbf{b}) + \text{ilr}(\varepsilon_i) \quad (1)$$

3. Results

3.1. Tree Crowns vs. Sparkleberry Clumps Distribution

Table 1 summarizes the values calculated for each of the burn units: the plot area, tree crown area, sparkleberry clumps area, and overlap area (intersection of tree crown area with sparkleberry clumps area). The proportion of area covered by tree crowns ranged from 0.37 in 24B Triangle to 0.77 in 24A Main; the sparkleberry cover was smaller, ranging from only 0.07 to 0.26. In five of the seven burn units, the proportion of overlap between the tree crowns and the sparkleberry was greater than 0.60 (Table 1), and the one-sided *t*-test indicated that the mean proportion (0.64) was significantly greater than 0.5 with a *p*-value of 0.03, which suggests that, on these plots, more sparkleberry occurred under the tree crowns instead of in an open canopy gap space.

Table 1. Area estimated from digitized sparkleberry shapefiles and tree crown shapefiles for each burn unit.

Burn Unit	Plot Area (m ²)	Tree Crown Area (m ²)	Tree Crown Area/Plot Area	Sparkleberry Area (m ²)	Sparkleberry Area/Plot Area	Overlap Area (m ²)	Overlap Area/Sparkleberry Area
16D1	1796.2	1218.2	0.67	416.2	0.23	303.1	0.72
16D5	1478.2	674.1	0.45	348.7	0.23	160.7	0.46
16D6	1860.5	754.3	0.40	245.0	0.13	90.5	0.37
24A Main	1342.5	1060.9	0.77	282.6	0.21	184.5	0.81
24A Triangle	873.2	574.2	0.50	227.6	0.26	159.9	0.71
24B Main	2242.0	1246.8	0.41	332.1	0.15	371.4	0.67
24B Triangle	838.7	586.6	0.37	56.3	0.07	58.4	0.75

3.2. Ground Truth Measurements

The ground truth estimates of sparkleberry cover were determined by multiplying the total area of the buffered polygons by the weighted mean of percentage cover and expressing the area as a proportion of the total plot area (Table 2). The *t*-test used to test the equality of the mean values for the digitized (0.139) and the ground truth (0.172) estimates was not significant (*p* = 0.53), meaning that the null hypothesis (the means were equal) was not rejected, which provides support for the digitized method.

Table 2. Proportional area of sparkleberry found in burn plots at Ft. Jackson, SC, based on ground truth versus digitized estimates of percent shrub cover.

Burn Unit	Digitized	Ground Truth
24A Main	0.137	0.211
24A Triangle	0.183	0.261
24B Main	0.166	0.148
24B Triangle	0.070	0.067

3.3. Shrub Fuel Loading Estimates

Shrub fuel density estimates were calculated using both the digitized sparkleberry shapefiles and the ground truth shapefiles for data extraction from the prefire, postfire, and consumption density rasters. The shrub fuel density estimates were multiplied by the area of sparkleberry coverage to estimate a quantity of fuel. Table 3 shows the estimated fuel quantities using the digitized sparkleberry and ground truth estimates, within areas of expected sparkleberry coverage (digitized sparkleberry or ground truth polygons) and outside areas of expected sparkleberry coverage. The area inside and outside of the polygons was calculated from the same shapefiles used to extract shrub fuel density values. The area of sparkleberry coverage from the ground truth measurements was calculated previously as the geometrically weighted mean times the polygon area, and is the same value used here. The area outside of the ground truth coverage is calculated as the total area minus the sparkleberry area.

Table 3. Estimated fuel loading (g/m²) from digitized and ground truth samples from inside digitized sparkleberry polygons.

Burn Unit	Preburn				Postburn			
	DIN	GIN	DOUT	GOUT	DIN	GIN	DOUT	GOUT
16D1	547		398		487		360	
16D5	700		488		563		350	
16D6	589		326		458		236	
24A Main	492	510	435	496	485	421	438	428
24A Triangle	585	550	521	496	569	514	495	521
24B Main	256	183	136	118	150	138	87	84
24B Triangle	211	135	254	123	198	277	232	253

DIN, DOUT, GIN, GOUT = inside and outside digitized polygons, inside and outside ground truth coverage, respectively.

As described above, 16D1, 16D5, and 16D6 did not have ground truth samples. All of the fitted linear regressions predicting ground truth shrub fuel loading from the digitized shrub fuel loading were significant (Table 4), therefore the fitted values were added to the fuel loading dataset used in subsequent analyses. None of the intercept terms were significantly different from zero, which suggested no systematic bias in the data. The fitted models accounted for more than 95 percent of the observed variation (Adj. R²), which increased confidence in the predicted ground truth shrub fuel loading for 16D1, 16D5, and 16D6.

Table 4. Summary of simple linear regression models used to estimate missing ground truth shrub fuel loading (g/m³) for small prescribed burns at Ft. Jackson, SC, burned in April 2018. “*” and “**” indicate that the estimated coefficient (intercept, slope) was significant at the 0.05 and 0.01 probability levels, respectively.

Model	Intercept	Slope	Pr > F	Adj. R ²	Estimated Fuel Loading		
					16D1	16D5	16D6
InsidePreburn	−110.54	1.18 **	0.009	0.97	533.8	714.9	584.0
OutsidePreburn	19.16	0.95 **	0.003	0.99	395.5	481.2	327.4
InsidePostBurn	−51.73	1.03 *	0.017	0.95	448.6	525.7	418.7
OutsidePostBurn	1.70	1.02 **	0.004	0.99	370.1	359.3	243.2

The general simple linear regression model was $GIN = \beta_0 + \beta_1DIN$ or $GOUT = \beta_0 + \beta_1DOUT$ for the preburn and postburn shrub fuel loadings.

3.4. Relationship between Fuel Consumption and Pyrolysis Gas Composition

Geometric mean pyrolysis gas concentrations determined by FTIR show the relative dominance of CO₂, CO, H₂O, and CH₄ in the composition as well as the variability in concentration values between burn units (Table 5). It is important to recall that the log-ratios between the gases contain relative information; analysis is underway to compare the measurements, which is outside the scope of the present work.

Table 5. Mean pyrolysis gas concentrations (ppm) derived from FTIR measurements for small, prescribed burns at Ft. Jackson, SC, in April 2018. Values are presented as the geometric mean (95 percent confidence interval).

Gas	Burn Unit				
	24B Main	24A Triangle	16D5	16D6	16D1
H ₂ O	243,741 ¹	19,839	10,073	8916	15,193
CO ₂	13,637	65,899	67,508	53,715	38,852
CO	2928	15,886	11,207	10,664	6546
CH ₄	306	1591	1261	1269	553
C ₂ H ₂	80	623	593	527	234
C ₂ H ₄	185	1013	822	657	340
C ₂ H ₆	24.6	100.8	55.9	52.0	28.0
Allene	2.4	18.2	15.7	12.4	6.1
C ₃ H ₆	27.3	181.3	113.7	85.0	48.8
C ₄ H ₆	4.2	72.6	41.9	26.8	15.8
Isobutene	0.6	14.6	8.7	3.8	2.7
Isoprene	0.7	41.5	12.2	3.5	2.8
CH ₃ OH	56.5	91.4	42.7	33.3	21.7
CH ₃ COOH	61.1	27.5	16.7	6.3	11.8
HCOOH	5.1	9.7	8.3	3.1	5.0
CH ₃ CHO	47.3	181.7	94.3	70.2	43.5
Acrolein	25.5	75.8	37.7	26.3	18.2
Acetone	21.6	48.7	25.0	19.1	13.3
HCHO	45.6	64.4	17.7	6.3	10.2
Furan	5.4	17.4	6.4	6.2	3.7
Furfural	13.1	21.9	7.5	8.0	5.5
Naphthalene	1.0	4.4	6.5	12.2	7.4
Methyl nitrite	6.1	10.5	3.4	4.3	8.1
HCN	20.1	92.7	103.4	86.3	51.2
HONO	4.6	1.8	0.6	0.8	1.7

¹ Geometric mean $\bar{x}_g = \sqrt[n]{\prod_{i=1}^n x_i}$ where x_i is each gas. Number of samples (n) by burn unit: 24BMain, 16D5 (1); 16D6 (2); 24A; Triangle, 16D1 (3).

Fuel consumption was calculated as the difference between pre- and postburn shrub fuel densities for both digitized and ground truth data. If estimated consumption was less than 0, it was assigned a value of 0. For 21 of the 24 tests, the Shapiro–Wilk test did not reject the hypothesis that the *ilr*-transformed gas concentrations were normally distributed based on the unadjusted probabilities. When adjusting the probabilities to control the false discovery rate, none of the Shapiro–Wilk probabilities were significant (p -value < 0.05) [57]. A summary of the four fitted models relating the pyrolysis gas composition to the fuel consumption is presented in Table 6. The F-statistic probabilities indicated that none of the models were significant, and the models accounted for less than 20 percent of the variation (R^2). Based on these results, there does not appear to be a direct relationship between fuel consumption and pyrolysis gas composition.

Table 6. Summary of simple linear models relating estimated fuel loading to composition of pyrolysis gases. None of the fitted models were significant.

Predictor	F-Statistic	Pr > F	R ²
Digitized Inside	0.30	0.83	0.09
Ground truth Inside	1.58	0.29	0.35
Digitized Outside	0.51	0.70	0.14
Ground truth Outside	0.32	0.83	0.10

4. Discussion and Conclusions

4.1. Tree Crowns vs. Sparkleberry Clumps Distribution

The distribution of sparkleberry clumps within each burn unit was expected to favor areas which did not fall under tree crowns, as the sparkleberry would then face competition for sunlight and soil nutrients. Assessing the chi-square results with an α -value of 0.05, only the burn units 16D1 and 24B main show a statistically significant association between sparkleberry distribution and crown cover; the remaining burn units do not show such an association. It is unclear whether the associations in 16D1 and 24B main indicate a higher proportion of sparkleberry located underneath or outside of tree crowns. Since the majority of burn units show no significant correlation between tree crown cover and sparkleberry clump location, it currently appears that sparkleberry distribution among the units is unrelated to the distribution of tree crowns, suggesting the species may be shade-tolerant, at least more so than previously assumed. That the distributions of tree crowns and understory shrub clumps are independent due to shade tolerance undermines any assumptions about understory shrub distributions that might otherwise be inferred from airborne remote sensing data, which is much more sensitive to overstory structure than that of the understory.

4.2. Ground Truth Measurements

The ground truth measurements provided a ground-based estimate of total sparkleberry coverage per burn unit. While the locations of sparkleberry bushes from the digitized sparkleberry clumps were determined with much higher resolution than the ground truth locations, the overall area of sparkleberry coverage from the independent estimates was assessed using *t*-tests. It was expected that there be no statistically significant difference between the ground truth measurements and the digitized sparkleberry, and this was confirmed. This supports our assertion that the burn units can be considered as replicates for interpreting our results, despite the lack of ground truth data at three of them.

4.3. Fuel Density/Consumption Estimates

When quantifying fuel consumption, it was expected that the fuel consumption would be greater within areas of sparkleberry coverage, as sparkleberry was delineated as the component of the fuel bed that can significantly increase fire behavior when conditions are favorable because the shrub crowns ignite resulting in larger flames. Personal communication, John Maitland, Chief, Forestry Branch, USAG Ft. Jackson to David Weise, 2015. While

sparkleberry was the focus of the present study, Wenk et al. [58] found similar results in another prescribed fire study in the Carolina sandhills in longleaf stands where turkey oak (*Quercus laevis*) was the dominant understory woody plant [59–62]. It is well-established that natural fuel loadings are highly variable, particularly in forested systems with an understory component [63–65]. This variability requires increased sample sizes in order to produce confidence intervals that do not include 0 if the arithmetic mean is used as was done in the present analysis. This problem associated with the arithmetic mean can be overcome by properly applying the geometric mean since fuels' data are compositional, similar to the gases [38]. With respect to the differences in consumption between regions of estimated sparkleberry as coverage, the regions of no coverage (outside of polygons) tended to have greater quantities of fuel prior to burning as well as greater estimates of fuel consumed, which is not expected, as areas within polygons are assumed to be fuel beds with sparkleberry shrubs which are consumed during burning, while areas outside of polygons are regarded as areas without sparkleberry. It is important to recall that the lack of sparkleberry coverage does not indicate that no fuel is present; litter, duff, and other herbaceous material account for a significant proportion of consumption [66,67]. Moreover, the areas designated as sparkleberry coverage are typically smaller than the areas outside of sparkleberry coverage. Even in burn units where mean fuel density was greater in areas of sparkleberry coverage than outside of sparkleberry coverage, the relative size of the areas was significant in determining the total fuel quantity, and the larger area outside of the sparkleberry coverage often determined that the total fuel quantity outside of sparkleberry coverage was greater than within coverage.

4.4. Relationship between Fuel Consumption and Pyrolysis Gas Composition

For the gas-phase data, the lack of a significant statistical relationship between fuel consumption and pyrolysis gas composition, while a novel finding, was not unexpected. By conservation of mass, the total yield of pyrolysis products is equivalent to the amount of wildland fuels that are heated and broken down into constituent materials and chemicals; thus, as more fuel is consumed, the total yield of pyrolysis gases increases. However, if heating efficiency and heating rate remain relatively constant, there is no reason to expect yield to increase or decrease on a per mass pyrolyzed basis. Similarly, the chemical makeup of the pyrolyzed fuels was fairly constant, therefore there was no expectation that the steady heating of constant fuels would produce a different composition of pyrolysis gases.

As the pyrolysis gases oxidize during combustion under similar conditions, the expectation is that the composition of the combustion products would be similar between the burn units. In the present study, fuel consumption was the difference between the starting and ending fuel mass; however, the amount of char and noncombustible silica ash were not included in the mass balance. If the amount of char and ash produced in these burns was assumed to be constant based on similar fuels and burning conditions, fuel consumption would not be affected by this omission. It is also well established that heating rates can affect the composition of pyrolysis products [68–70]. For these prescribed fire experiments, the heating rates produced by a wildland flame are in the order of $100 \text{ s of } ^\circ\text{C s}^{-1}$, which falls in the range of fast pyrolysis, and were similar [71]. Therefore, given the relatively similar burning conditions and fuels, no relationship between pyrolysis gas composition and fuel consumption is expected. Nevertheless, this is a novel finding based on a limited sampling of pyrolysis gases in a single fuel type. Although our focus was on a single shrub species, it comprised only a small fraction of the fuels consumed in these fires [27], which undoubtedly also contributed to pyrolysis gas emissions. It would be worthwhile to measure pyrolysis gas emissions in relation to consumption at other sites and in other fuel types.

Author Contributions: Conceptualization, D.R.W. and J.S.M.; methodology, A.T.H.; software, B.C.B. and J.L.B.; validation, D.R.W. and T.J.J.; formal analysis, M.M.H., A.T.H., D.R.W., B.C.B., J.L.B. and A.K.; investigation, D.R.W., A.M.B., R.G.T., C.A.B. and T.L.M.; resources, J.S.M.; data curation, M.M.H., A.T.H. and J.S.M.; writing—original draft preparation, M.M.H., A.T.H., D.R.W., A.M.B., T.L.M., B.C.B. and T.J.J.; writing—review and editing, M.M.H., A.T.H., D.R.W., A.M.B., R.G.T., C.A.B., T.L.M., B.C.B., J.L.B., A.K. and T.J.J.; supervision, D.R.W., A.T.H., R.G.T., T.L.M., J.S.M. and T.J.J.; project administration, D.R.W.; funding acquisition, D.R.W. All authors have read and agreed to the published version of the manuscript.

Funding: This research has been supported by the Department of Defense Strategic Environmental Research and Development Program (grant No. RC-2460).

Institutional Review Board Statement: Not applicable.

Informed Consent Statement: Not applicable.

Acknowledgments: The authors would like to thank the forestry team from Fort Jackson, South Carolina for assisting on this project at every stage. This study was completed under Department of Defense's Strategic Environmental Research and Development Program (SERDP) Project RC-2640 and we thank them for the support. PNNL is operated by the U.S. Department of Energy by the Battelle Memorial Institute under contract DE-AC06-76RLO1830.

Conflicts of Interest: The authors declare no conflict of interest.

References

1. Scott, A.C.; Bowman, D.M.; Bond, W.J.; Pyne, S.J.; Alexander, M.E. *Fire on Earth: An Introduction*; John Wiley & Sons: Hoboken, NJ, USA, 2013.
2. Hiers, J.K.; O'Brien, J.J.; Varner, J.M.; Butler, B.W.; Dickinson, M.; Furman, J.; Gallagher, M.; Godwin, D.; Goodrick, S.L.; Hood, S.M. Prescribed fire science: The case for a refined research agenda. *Fire Ecol.* **2020**, *16*, 11. [\[CrossRef\]](#)
3. Pyne, S.J. *The Pyrocene: How We Created an Age of Fire, and What Happens Next*; University of California Press: Oakland, CA, USA, 2021.
4. Crutzen, P.J.; Heidt, L.E.; Krasnec, J.P.; Pollock, W.H.; Seiler, W. Biomass burning as a source of atmospheric gases CO, H₂, N₂O, NO, CH₃Cl and COS. *Nature* **1979**, *282*, 253–256. [\[CrossRef\]](#)
5. Burling, I.; Yokelson, R.J.; Griffith, D.W.; Johnson, T.J.; Veres, P.; Roberts, J.; Warneke, C.; Urbanski, S.; Reardon, J.; Weise, D. Laboratory measurements of trace gas emissions from biomass burning of fuel types from the southeastern and southwestern United States. *Atmos. Chem. Phys.* **2010**, *10*, 11115–11130. [\[CrossRef\]](#)
6. Eck, T.; Holben, B.; Reid, J.; O'Neill, N.; Schafer, J.; Dubovik, O.; Smirnov, A.; Yamasoe, M.; Artaxo, P. High aerosol optical depth biomass burning events: A comparison of optical properties for different source regions. *Geophys. Res. Lett.* **2003**, *30*. [\[CrossRef\]](#)
7. Yokelson, R.J.; Susott, R.; Ward, D.E.; Reardon, J.; Griffith, D.W. Emissions from smoldering combustion of biomass measured by open-path Fourier transform infrared spectroscopy. *J. Geophys. Res. Atmos.* **1997**, *102*, 18865–18877. [\[CrossRef\]](#)
8. Radke, L.F.; Hegg, D.A.; Hobbs, P.V.; Nance, J.D.; Lyons, J.H.; Laursen, K.K.; Weiss, R.E.; Riggan, P.J.; Ward, D.E. Particulate and trace gas emissions from large biomass fire in North America. In *Global Biomass Burning: Atmospheric, Climatic, and Biospheric Implications*; Levine, J.S., Ed.; The MIT Press: Cambridge, MA, USA, 1991; pp. 209–216.
9. Rein, G. Smouldering combustion phenomena in science and technology. *Int. Rev. Chem. Eng.* **2009**, *1*, 3–18.
10. Collard, F.-X.; Blin, J. A review on pyrolysis of biomass constituents: Mechanisms and composition of the products obtained from the conversion of cellulose, hemicelluloses and lignin. *Renew. Sustain. Energy Rev.* **2014**, *38*, 594–608. [\[CrossRef\]](#)
11. Akagi, S.; Yokelson, R.J.; Wiedinmyer, C.; Alvarado, M.; Reid, J.; Karl, T.; Crounse, J.; Wennberg, P. Emission factors for open and domestic biomass burning for use in atmospheric models. *Atmos. Chem. Phys.* **2011**, *11*, 4039–4072. [\[CrossRef\]](#)
12. Yokelson, R.J.; Burling, I.; Gilman, J.; Warneke, C.; Stockwell, C.; De Gouw, J.; Akagi, S.; Urbanski, S.; Veres, P.; Roberts, J. Coupling field and laboratory measurements to estimate the emission factors of identified and unidentified trace gases for prescribed fires. *Atmos. Chem. Phys.* **2013**, *13*, 89–116. [\[CrossRef\]](#)
13. Rein, G. Smouldering Fires and Natural Fuels. In *Fire Phenomena and the Earth System: An Interdisciplinary Guide to Fire Science*, 1st ed.; Belcher, C.M., Ed.; John Wiley & Sons: Oxford, UK, 2013; pp. 15–33.
14. Bostrom, D.; Skoglund, N.; Grimm, A.; Boman, C.; Ohman, M.; Brostrom, M.; Backman, R. Ash transformation chemistry during combustion of biomass. *Energy Fuels* **2012**, *26*, 85–93. [\[CrossRef\]](#)
15. Qu, Z.; Schmidt, F.M. In situ H₂O and temperature detection close to burning biomass pellets using calibration-free wavelength modulation spectroscopy. *Appl. Phys. B* **2015**, *119*, 45–53. [\[CrossRef\]](#)
16. Yokelson, R.J.; Griffith, D.W.; Ward, D.E. Open-path Fourier transform infrared studies of large-scale laboratory biomass fires. *J. Geophys. Res. Atmos.* **1996**, *101*, 21067–21080. [\[CrossRef\]](#)

17. Scharko, N.K.; Oeck, A.M.; Tonkyn, R.G.; Baker, S.P.; Lincoln, E.N.; Chong, J.; Corcoran, B.M.; Burke, G.M.; Weise, D.R.; Myers, T.L. Identification of gas-phase pyrolysis products in a prescribed fire: First detections using infrared spectroscopy for naphthalene, methyl nitrite, allene, acrolein and acetaldehyde. *Atmos. Meas. Tech.* **2019**, *12*, 763–776. [[CrossRef](#)]
18. Akagi, S.K.; Burling, I.R.; Mendoza, A.; Johnson, T.J.; Cameron, M.; Griffith, D.W.; Paton-Walsh, C.; Weise, D.R.; Reardon, J.; Yokelson, R.J. Field measurements of trace gases emitted by prescribed fires in southeastern US pine forests using an open-path FTIR system. *Atmos. Chem. Phys.* **2014**, *14*, 199–215. [[CrossRef](#)]
19. Burling, I.; Yokelson, R.J.; Akagi, S.; Urbanski, S.; Wold, C.E.; Griffith, D.W.; Johnson, T.J.; Reardon, J.; Weise, D. Airborne and ground-based measurements of the trace gases and particles emitted by prescribed fires in the United States. *Atmos. Chem. Phys.* **2011**, *11*, 12197–12216. [[CrossRef](#)]
20. Gilman, J.; Lerner, B.; Kuster, W.; Goldan, P.; Warneke, C.; Veres, P.; Roberts, J.; De Gouw, J.; Burling, I.; Yokelson, R. Biomass burning emissions and potential air quality impacts of volatile organic compounds and other trace gases from fuels common in the US. *Atmos. Chem. Phys.* **2015**, *15*, 13915–13938. [[CrossRef](#)]
21. Andreae, M.O.; Merlet, P. Emission of trace gases and aerosols from biomass burning. *Glob. Biogeochem. Cycles* **2001**, *15*, 955–966. [[CrossRef](#)]
22. Koss, A.R.; Sekimoto, K.; Gilman, J.B.; Selimovic, V.; Coggon, M.M.; Zarzana, K.J.; Yuan, B.; Lerner, B.M.; Brown, S.S.; Jimenez, J.L. Non-methane organic gas emissions from biomass burning: Identification, quantification, and emission factors from PTR-ToF during the FIREX 2016 laboratory experiment. *Atmos. Chem. Phys.* **2018**, *18*, 3299–3319. [[CrossRef](#)]
23. Scharko, N.K.; Oeck, A.M.; Myers, T.L.; Tonkyn, R.G.; Banach, C.A.; Baker, S.P.; Lincoln, E.N.; Chong, J.; Corcoran, B.M.; Burke, G.M.; et al. Gas-phase pyrolysis products emitted by prescribed fires in pine forests with a shrub understory in the southeastern United States. *Atmos. Chem. Phys.* **2019**, *19*, 9681–9698. [[CrossRef](#)]
24. Weise, D.R.; Fletcher, T.H.; Johnson, T.J.; Hao, W.; Diitenberger, M.; Princevac, M.; Butler, B.; McAllister, S.; O'Brien, J.; Loudermilk, L. A project to measure and model pyrolysis to improve prediction of prescribed fire behavior. In *Advances in Forest Fire Research 2018*; Viegas, D.X., Ed.; University of Coimbra: Coimbra, Portugal, 2018; pp. 308–318.
25. Ottmar, R.D.; Sandberg, D.V.; Riccardi, C.L.; Prichard, S.J. An overview of the fuel characteristic classification system—quantifying, classifying, and creating fuelbeds for resource planning. *Can. J. For. Res.* **2007**, *37*, 2383–2393. [[CrossRef](#)]
26. Boyer, W.D. *Techniques and Methods of Measuring Understory Vegetation. Proceedings of a Symposium on Forest Fire Research at Tifton, Georgia*; Southern Forest Experiment Station: Tifton, GA, USA, 1959.
27. Hudak, A.T.; Kato, A.; Bright, B.C.; Loudermilk, E.L.; Hawley, C.; Restaino, J.C.; Ottmar, R.D.; Prata, G.A.; Cabo, C.; Prichard, S.J. Towards spatially explicit quantification of pre-and postfire fuels and fuel consumption from traditional and point cloud measurements. *For. Sci.* **2020**, *66*, 428–442. [[CrossRef](#)]
28. Banach, C.A.; Bradley, A.M.; Tonkyn, R.G.; Williams, O.N.; Chong, J.; Weise, D.R.; Myers, T.L.; Johnson, T.J. Dynamic infrared gas analysis from longleaf pine fuel beds burned in a wind tunnel: Observation of phenol in pyrolysis and combustion phases. *Atmos. Meas. Tech.* **2021**, *14*, 2359–2376. [[CrossRef](#)]
29. Christensen, N.L. Vegetation of the Southeastern Coastal Plain, in North American Terrestrial Vegetation. In *Northern American Terrestrial Vegetation*, 2nd ed.; Billings, M.G.B.W.D., Ed.; Cambridge University Press: New York, NY, USA, 2000.
30. Jackson, J. Red-cockaded Woodpecker (*Dryobates borealis*), version 1.0. In *Birds of the World*; Poole, A.F., Gill, F.B., Eds.; Cornell Lab of Ornithology: Ithaca, NY, USA, 2020.
31. Silva, C.A.; Hudak, A.T.; Vierling, L.A.; Loudermilk, E.L.; O'Brien, J.J.; Hiers, J.K.; Jack, S.B.; Gonzalez-Benecke, C.; Lee, H.; Falkowski, M.J. Imputation of individual longleaf pine (*Pinus palustris* Mill.) tree attributes from field and LiDAR data. *Can. J. Remote Sens.* **2016**, *42*, 554–573. [[CrossRef](#)]
32. Hudak, A.T.; Bright, B.C.; Pokswinski, S.M.; Loudermilk, E.L.; O'Brien, J.J.; Hornsby, B.S.; Klaueberg, C.; Silva, C.A. Mapping forest structure and composition from low-density LiDAR for informed forest, fuel, and fire management at Eglin Air Force Base, Florida, USA. *Can. J. Remote Sens.* **2016**, *42*, 411–427. [[CrossRef](#)]
33. Hudak, A.T.; Evans, J.S.; Stuart Smith, A.M. LiDAR utility for natural resource managers. *Remote Sens.* **2009**, *1*, 934–951. [[CrossRef](#)]
34. Ullman, S. *The Interpretation of Visual Motion*; Massachusetts Inst of Technology: Cambridge, MA, USA, 1979; Volume 203, pp. 405–426.
35. Hillman, S.; Wallace, L.; Reinke, K.; Hally, B.; Jones, S.; Saldias, D.S. A method for validating the structural completeness of understory vegetation models captured with 3D remote sensing. *Remote Sens.* **2019**, *11*, 2118. [[CrossRef](#)]
36. Mathews, B.J.; Strand, E.K.; Smith, A.M.; Hudak, A.T.; Dickinson, B.; Kremens, R.L. Laboratory experiments to estimate interception of infrared radiation by tree canopies. *Int. J. Wildland Fire* **2016**, *25*, 1009–1014. [[CrossRef](#)]
37. R Core Team. *R: A Language and Environment for Statistical Computing*; R Foundation for Statistical Computing: Vienna, Austria, 2021.
38. Weise, D.R.; Hao, W.M.; Baker, S.; Princevac, M.; Aminfar, A.-H.; Palarea-Albaladejo, J.; Ottmar, R.D.; Hudak, A.T.; Restaino, J.; O'Brien, J.J. Comparison of fire-produced gases from wind tunnel and small field experimental burns. *Int. J. Wildland Fire* **2022**, *31*, 409–434. [[CrossRef](#)]
39. Griffith, D.W.T. MALT5 User Guide Version 5.5.9. Wollongong, NSW, Australia. 2016. Available online: <https://software-ab.informatik.uni-tuebingen.de/download/malt/welcome.html> (accessed on 15 July 2022).
40. Sharpe, S.W.; Johnson, T.J.; Sams, R.L.; Chu, P.M.; Rhoderick, G.C.; Johnson, P.A. Gas-phase databases for quantitative infrared spectroscopy. *Appl. Spectrosc.* **2004**, *58*, 1452–1461. [[CrossRef](#)]

41. Gordon, I.E.; Rothman, L.S.; Hill, C.; Kochanov, R.V.; Tan, Y.; Bernath, P.F.; Birk, M.; Boudon, V.; Campargue, A.; Chance, K. The HITRAN2016 molecular spectroscopic database. *J. Quant. Spectrosc. Radiat. Transf.* **2017**, *203*, 3–69. [[CrossRef](#)]
42. USDA NRCS. The PLANTS Database. Available online: <http://plants.usda.gov> (accessed on 15 July 2022).
43. NC State Extension. North Carolina Extension Gardener Plant Toolbox. Available online: <https://plants.ces.ncsu.edu/> (accessed on 23 February 2022).
44. De Winter, J.C. Using the Student's t-test with extremely small sample sizes. *Pract. Assess. Res. Eval.* **2013**, *18*, 10.
45. Aitchinson, J. *The Statistical Analysis of Compositional Data. Monographs on Statistics and Applied Probability*; Chapman and Hall: London, UK; New York, NY, USA, 1986.
46. Weise, D.R.; Palarea-Albaladejo, J.; Johnson, T.J.; Jung, H. Analyzing wildland fire smoke emissions data using compositional data techniques. *J. Geophys. Res. Atmos.* **2020**, *125*, e2019JD032128. [[CrossRef](#)]
47. Weise, D.R.; Fletcher, T.H.; Safdari, M.-S.; Amini, E.; Palarea-Albaladejo, J. Application of compositional data analysis to determine the effects of heating mode, moisture status and plant species on pyrolysates. *Int. J. Wildland Fire* **2021**, *31*, 24–45. [[CrossRef](#)]
48. Weise, D.R.; Jung, H.; Palarea-Albaladejo, J.; Cocker, D.R. Compositional data analysis of smoke emissions from debris piles with low-density polyethylene. *J. Air Waste Manag. Assoc.* **2020**, *70*, 834–845. [[CrossRef](#)]
49. Egozcue, J.J.; Pawłowsky-Glahn, V.; Mateu-Figueras, G.; Barcelo-Vidal, C. Isometric logratio transformations for compositional data analysis. *Math. Geol.* **2003**, *35*, 279–300. [[CrossRef](#)]
50. Palarea-Albaladejo, J.; Martín-Fernández, J.A.; Buccianti, A. Compositional methods for estimating elemental concentrations below the limit of detection in practice using R. *J. Geochem. Explor.* **2014**, *141*, 71–77. [[CrossRef](#)]
51. Palarea-Albaladejo, J.; Martín-Fernández, J.A. zCompositions—R package for multivariate imputation of left-censored data under a compositional approach. *Chemom. Intell. Lab. Syst.* **2015**, *143*, 85–96. [[CrossRef](#)]
52. McNaught, A.D.; Wilkinson, A. *Compendium of Chemical Terminology*; Blackwell Science: Oxford, UK, 1997; Volume 1669.
53. Oksanen, J.; Blanchet, F.G.; Friendly, M.; Kindt, R.; Wagner, H.H. *Vegan: Community Ecology Package. R Package Version 2.5-7*; R Welthandelsplatz 1: Vienna, Austria, 2020.
54. Anderson, M.J. A new method for non-parametric multivariate analysis of variance. *Austral Ecol.* **2001**, *26*, 32–46.
55. Van den Boogaart, K.G.; Tolosana-Delgado, R. *Analyzing Compositional Data with R*; Springer: Berlin/Heidelberg, Germany, 2013; Volume 122.
56. Anderson, M.J. Permutational Multivariate Analysis of Variance (PERMANOVA). In *Wiley StatsRef: Statistics Reference Online*; John Wiley & Sons: Hoboken, NJ, USA, 2014; pp. 1–15.
57. Benjamini, Y.; Hochberg, Y. Controlling the false discovery rate: A practical and powerful approach to multiple testing. *J. R. Stat. Soc. Ser. B* **1995**, *57*, 289–300. [[CrossRef](#)]
58. Wenk, E.S.; Wang, G.G.; Walker, J.L. Within-stand variation in understorey vegetation affects fire behaviour in longleaf pine xeric sandhills. *Int. J. Wildland Fire* **2011**, *20*, 866–875. [[CrossRef](#)]
59. Lozano, J.S. *An Investigation of Surface and Crown Fire Dynamics in Shrub Fuels*; University of California: Riverside, CA, USA, 2011.
60. Tachajapong, W.; Lozano, J.; Mahalingam, S.; Weise, D.R. Experimental modelling of crown fire initiation in open and closed shrubland systems. *Int. J. Wildland Fire* **2014**, *23*, 451–462. [[CrossRef](#)]
61. Marino, E.; Guijarro, M.; Madrigal, J.; Hernando, C.; Diez, C. Assessing fire propagation empirical models in shrub fuel complexes using wind tunnel data. *WIT Trans. Ecol. Environ.* **2008**, *119*, 121–130.
62. Cobian-Iñiguez, J.; Aminfar, A.; Weise, D.R.; Princevac, M. On the Use of Semi-empirical Flame Models for Spreading Chaparral Crown Fire. *Front. Mech. Eng.* **2019**, *5*, 50. [[CrossRef](#)]
63. Keane, R.E.; Gray, K.; Bacciu, V. *Spatial Variability of Wildland Fuel Characteristics in Northern Rocky Mountain Ecosystems*; Research Paper RMRS-RP-98; USDA Forest Service, Rocky Mountain Research Station: Fort Collins, CO, USA, 2012; Volume 98, 56p.
64. Parresol, B.R.; Blake, J.I.; Thompson, A.J. Effects of overstorey composition and prescribed fire on fuel loading across a heterogeneous managed landscape in the southeastern USA. *For. Ecol. Manag.* **2012**, *273*, 29–42. [[CrossRef](#)]
65. Skowronski, N.; Clark, K.; Nelson, R.; Hom, J.; Patterson, M. Remotely sensed measurements of forest structure and fuel loads in the Pinelands of New Jersey. *Remote Sens. Environ.* **2007**, *108*, 123–129. [[CrossRef](#)]
66. Ottmar, R.D.; Hudak, A.T.; Prichard, S.J.; Wright, C.S.; Restaino, J.C.; Kennedy, M.C.; Vihnanek, R.E. Pre-fire and post-fire surface fuel and cover measurements collected in the south-eastern United States for model evaluation and development—RxCADRE 2008, 2011 and 2012. *Int. J. Wildland Fire* **2015**, *25*, 10–24. [[CrossRef](#)]
67. Hudak, A.T.; Dickinson, M.B.; Bright, B.C.; Kremens, R.L.; Loudermilk, E.L.; O'Brien, J.J.; Hornsby, B.S.; Ottmar, R.D. Measurements relating fire radiative energy density and surface fuel consumption—RxCADRE 2011 and 2012. *Int. J. Wildland Fire* **2015**, *25*, 25–37. [[CrossRef](#)]
68. Demirbas, A.; Arin, G. An overview of biomass pyrolysis. *Energy Sour.* **2002**, *24*, 471–482. [[CrossRef](#)]
69. Kan, T.; Strezov, V.; Evans, T.J. Lignocellulosic biomass pyrolysis: A review of product properties and effects of pyrolysis parameters. *Renew. Sustain. Energy Rev.* **2016**, *57*, 1126–1140. [[CrossRef](#)]
70. Hajaligol, M.R.; Howard, J.B.; Longwell, J.P.; Peters, W.A. Product compositions and kinetics for rapid pyrolysis of cellulose. *Ind. Eng. Chem. Process Des. Dev.* **1982**, *21*, 457–465. [[CrossRef](#)]
71. Butler, B.; Cohen, J.; Latham, D.; Schuette, R.; Sopko, P.; Shannon, K.; Jimenez, D.; Bradshaw, L. Measurements of radiant emissive power and temperatures in crown fires. *Can. J. For. Res.* **2004**, *34*, 1577–1587. [[CrossRef](#)]